PCCP

Accepted Manuscript

ROYAL SOCIETY OF CHEMISTRY

www.rsc.org/pccp

The theoretical investigation on the 4-(4-phenyl-4-α-naphthylbutadieny)-triphenylamine derivatives as hole transporting materials of perovskites-type solar cells

Wei-Jie Chi[ab] and Ze-Sheng Li*[abcd]

[a] *School of Chemistry, Beijing Institute of Technology, Beijing 100081, China.*

[b] *Key Laboratory of Cluster Science of Ministry of Education, China*

[c] *Beijing Key Laboratory for Chemical Power Source and Green Catalysis, China*

[d] *The Academy of Fundamental and Interdisciplinary Sciences, Harbin Institute of Technology, Harbin 150080, China.*

* *E-mail: zeshengli@bit.edu.cn*

Abstract The electronic structures, optical properties and hole mobilities of 4-(4-phenyl-4-α-naphthylbutadieny) -triphenylamine and its five derivatives are investigated by density functional theory (DFT). The results show that the highest occupied molecular orbital (HOMO) of all molecules are almost fully delocalized throughout the whole molecule, and the substituents -$N(CH_3)_2$ and -C_6H_5 denoted as molecules 6 and 2 respectively, have the large contribution to HOMO, which is favorable for hole transfer integral and hole mobility. Spectrum analysis indicates that all molecules have large Stokes shift based on absorption and emission spectrum. In addition, it is found that the hole reorganization energy of all molecules is about 0.5 times compared with that of electrons, which implies that hole mobility will bigger than electron mobility. On the basis of predicted packing motifs, the hole mobilities (u) of all molecules are also obtained. The largest hole mobility of molecule 2 (0.1063 $cm^2v^{-1}s^{-1}$) exhibits higher than that of other molecules due to face-to-face stacking mode, which suggests that -C_6H_5 is a well substituent group for improving hole mobility compared with other electron releasing groups. We hope that our results will be helpful for the further rational molecular design and synthesis of novel hole transport materials (HTMs) for high performance perovskites-type solar cells.

Keywords Charge transport; Hole mobility; perovskites solar cells; Density functional theory

1. Introduction

Organic-inorganic halide perovskites have received increasing attention beginning with their incorporation as sensitizers into dye-sensitized solar cells by Miyasaka el at in 2009[1]. A significant efficiency of 3.81% was obtained from $CH_3NH_3PbI_3$ with photocurrent onset from ~800 nm. This work opened a new frontier in the development of solar energy harvesting technologies. The perovskites-type solar cells represent a new class of electrochemical solar cells based on sensitized mesoporous TiO2 and a liquid electrolyte in sandwith-like architecture. In 2011, N.G. Park and coworkers[2] obtained an efficiency of 6.54% through a careful optimization of the mesoporous layer thickness, perovskite concentration and surface treatment. Despite the efficiencies achieved in such configurations, the overall instability of the solar cells due to the dissolution of the perovskite in the liquid electrolyte appeared to be a challenge. In 2012, N.G. Park, M. Grätzel and coworkers[3, 4] achieved a breakthrough in both efficiency and stability through utilization of a solid-state hole transporter 2,2′,7,7′- tetrakis (N,N-p-dimethoxy-phenylamino) - 9, 9′ - spirobifluorene (spiro-OMeTAD) with $CH_3NH_3PbI_3$ and $CH_3NH_3PbI_{3-x}Cl_x$ light absorbers. Extremely rapid progress was made during 2013 with energy conversion efficiencies reaching a confirmed 16.2% by using the mixed-halide $CH_3NH_3PbI_{3-x}Br_x$ (10–15% Br) and a poly-triarylamine HTMs (S. I. Seok, personal communication) at the end of year. In early 2014, an overall power conversion efficiency (PCE) of 16.7% was obtained based on mesoporous (mp)-TiO2/ $CH_3NH_3PbI_3$/HTM/Au solar cell, and the PCE is the highest value reported for perovskite-based solar cells to date with

spiro-OMeTAD[5].

To date, perovskite-type solar cells with and without HTM have been developed, the perovskite solar cells without HTM exhibit a PCE of just over 10%[6]. This is because HTM plays a key role in hole-transportation and retardation of charge recombination. So far, typical HTMs have spiro-OMeTAD, poly-triarylamine (PTAA), and poly (3-hexylthiophene) (P_3HT), and so on. Although spiro-OMeTAD continues to be the best performing candidate of HTM, the high cost of spiro-OMeTAD impedes the growth and advancement of high efficiency cost-effective perovskite solar cells. So, it is important and urgent that study on mechanism of hole transport and development new HTMs with good hole mobility, a compatible HOMO energy level relative to organolead halide perovskites and low cost for commercialization from experiment and theoretical level. Recently, some excellent HTMs have been synthesized and characterized. Such as, Prof. Xudong Yang and coworkers synthesized tetrathiafulvalene (TTF-1) and compared to cells on the well-known doping spiro-OMeTAD, perovskite solar cells based on dopant – free TTF-1 performed a comparable efficiency of 11.03%[7]. Prof. Mohammad Khaja Nazeeruddin group designed and synthesized a new HTM called Fused-F in their paper, the device based on this new material achieved high PCE of 12.8% under the illumination of 98.8mW cm^{-1}, which was better than the well-known spiro-OMeTAD under the same conditions[8]. Prof. Subodh G. Mhaisalkar group also synthesized three novel new hole-conducting molecules (called T101, T102, and T103) based on a triptycence core, and the mesoporous perovskite solar cells fabricated using T102 and T103 as the

HTMs showed a PCE of 12.24% and 12.38%, respectively, which is comparable to that obtained using the best performing HTM spiro–OMeTAD[9]. Two new triphenylamine-based HTMs were employed in $CH_3NH_3PbI_3$ perovskite solar cells, and the 11.63% of PCE has been achieved by Qingbo Meng group[10], and their typical advantages are easy synthesis, low cost and relatively good cell performance, which indicated that 4-(4-phenyl-4-α-naphthylbutadieny)-triphenylamine (Figure 1, named (1)) is excellent parent molecule for HTMs. To our knowledge, although a large number of experimental works have been performed about new HTMs, the report of the theoretical study about HTM based on perovskite solar cells has not been found up to now.

As is well konwn, triphenylamine (TPA) derivatives have been widely used in HTMs because of its efficient hole mobilities. In the present study, different electron releasing substituent groups (-C_6H_5, -CH_3, -OH, -OCH_3, and -$N(CH_3)_2$) are introduced into 4-(4-phenyl-4-α-naphthylbutadieny)-triphenylamine skeleton to design some new potential HTMs (see Figure 1). We focus on the effects of different donor group on molecular orbitals, absorption and emission properties, and hole transport behavior in order to look for excellent HTM with high hole mobility to further develop efficient perovskites-type solar cells. The structural, electronic and optical properties, and hole transport properties of these new HTMs are first predicted and characterized by density function theory (DFT). We hope that the results can provide a useful help for the synthetic study and reasonable design of high performance HTMs with high hole mobility, and also hope that it can be

applied to organic-inorganic halide perovskites solar cells.

2. Computational methods

Density functional theory (DFT) were employed to optimize the ground state based functional B3LYP with base set 6-31G(d,p), which can provide more accurate description for neutral states in extended π-conjugated systems[11]. All optimized geometries show no imaginary frequency, which ensures energetic minima. All the calculations were performed using the Gaussian 09 software package[12]. The absorption spectra and corresponding excitation energies were evaluated using the time-dependent density functional theory (TD-DFT) based on coulomb-attenuating method CAM-B3LYP/6-31G(d,p) [13]. The solvent effects were also taken into consideration here using the conductor-like polarizable continuum model (C-PCM) with the dielectric constants of chlorobenzene (ε=5.6968).

There are mainly two mechanisms describing carrier transport in organic semiconductors, namely, the band model and the hopping model [14, 15]. In inorganic semiconductors, charge transport is governed by the energy band, due to strong covalent interactions. However, in many cases, the charge transport of organic semiconductors can be well described with the thermally activated hopping and diffusion model since they are have weak intermolecular electronic coupling (reorganization energy> transfer integral)[16-20]. So in this study, we can deal with the charge transport process by the semi-classical Marcus theory [21], and the charge hopping rate (k) is expressed as:

$$k = \frac{4\pi^2}{h} v^2 \frac{1}{\sqrt{4\pi\lambda k_B T}} exp\left[-\frac{\lambda}{4k_B T} \right] \qquad (1)$$

where v is the transfer integral, λ is the reorganization energy, h is the Planck constant, T is the temperature in Kelvin, and k_B is the Boltzmann constant, respectively.

In generally, the λ can be estimated by the adiabatic potential energy surface approach [22, 23].

$$\lambda = \lambda_0 + \lambda_{+/-} = (E_0^* - E_0) + (E_{+/-}^* - E_{+/-}) \quad (2)$$

E_0 and $E_{+/-}$ respectively represent the energies of neutral and charged species in their lowest energy geometries, while E_0^* and $E_{+/-}^*$ are respectively the energies of the neutral molecule with charged geometry and charged molecule with the ground state geometry.

To achieve high carrier mobility, the λ needs to be minimized, and the v needs to be maximized. The v, which measures the strength of electronic coupling between the donor and acceptor states, depends on the relative arrangement of the molecule in the solid state[24]. In this work, we adopt a direct approach to investigate the charge transport properties [25, 26], which can be written as

$$V = \left\langle \Psi_i^{HOMO/LUMO} \middle| F \middle| \Psi_f^{HOMO/LUMO} \right\rangle \quad (3)$$

where F is the Fock operator, Ψ_i and Ψ_f represent the frontier orbitals of molecules 1 and 2 respectively in the dimer. The superscripts denote the frontier orbitals in which the charge hopping occurs, which are mostly at the HOMO level for holes and the LUMO level for electrons.

Assuming a Brownian motion of charge carrier in the absence of applied electric field, electron mobility can be calculated from the diffusion coefficient D with the Einstein equation[27].

$$\mu = \frac{eD}{k_B T} \qquad (4)$$

where e is the charge, D is the diffusion coefficient which can be approximately evaluated as[28].

$$D = \frac{1}{2d}\sum_i r_i^2 k_i P_i \qquad (5)$$

where i is a given transfer pathway and r_i represents the charge hopping centroid to centroid distance, d is to 3 since the diffusion is regarded in three dimension for compounds investigated and P_i ($P_i = k_i / \sum_i k_i$) is the relative probability for charge hopping to the ith pathway.

Crystal structure prediction was performed for molecules 1 - 6 by using the polymorph predictor module in Materials Studio[29], the single molecule was optimized by DMol3 module and electrostatic potential charges of all atoms were obtained. Then the crystal structure prediction was carried out by employing PBE functional and the Dreiding force field[30], which was considered to be more appropriate force fields for molecular crystal prediction [31]. For molecules 1 - 6, the polymorph predictor calculations are restricted to the five most probable space group, $P2_1/C$, P-1, $P2_12_12_1$, $P2_1$, and C2/C [32]. We sorted the obtained crystal structures in term of their total energies. Finally, crystal structures of molecules 1 – 6 with the lowest energies were selected for further DFT calculations on their hole mobilities.

3. Results and discussion

3.1 Frontier molecular orbital

It is useful to examine the frontier molecular orbitals (FMOs) of molecules under investigation. The FMO is one of key factor to illustrate the carrier transport

properties, and the calculated FMOs of molecules 1-6 are shown in Figure 2. From Figure 2, this gives an indication that both the HOMO and the lowest unoccupied molecular orbital (LUMO) possess π features. The HOMOs of molecules 1 - 5 spread over the whole molecule, while the HOMO of molecule 6 is localized on the phenylamine unit. The LUMOs of molecules 1, 2, 4 - 6 mainly localize at 4-phenyl-4-α-naphthylbutadienyl unit, while LUMO of molecule 3 mostly distributes to phenylamine unit. In other words, their HOMOs are almost fully delocalized while their LUMO are not fully delocalized throughout the whole molecule. The good HOMO delocalization is favorable for hole transport and hole transfer integral. The result of FMOs analysis suggests that all of the six molecules have well hole transport property, they are potential candidates as HTMs.

Another way to understand the influence of the electronic properties is to analyze the HOMO energy (E_{HOMO}), LUMO energy (E_{LUMO}) and energy gap (Δ_{H-L}) values. Here, our calculated Δ_{H-L} is the orbital energy difference between HOMO and LUMO. The calculated and experimental data are listed in Table 1. From Table 1, we can see that the calculated E_{HOMO} of 3 and 4 are -4.76 and -4.65 eV, respectively, while the corresponding experimental values are -5.35 and -5.23 eV. This result suggests that although we can not obtain accurate E_{HOMO} by DFT, the changing trend of between calculated and experimental values of E_{HOMO} is consistent. Moreover, the same trend can also be found in E_{LUMO} and Δ_{H-L}. The contrastive result shows that our calculation method is reliable. From Table 1, it is clearly to see that the E_{HOMO} is in the order of 6=4>5>3>2>1, the sequence of E_{LUMO} is 6>5=4>1>3>2. Thus, one can find that the

compounds with stronger donor groups (-OCH_3, OH, and -$N(CH_3)_2$) have higher E_{HOMO} and E_{LUMO} than those compounds with weaker donor groups (-H, -C_6H_5, and -CH_3). The sequence of Δ_{H-L} is 1>6>2=3>5>4. These results indicate that the E_{HOMO}, E_{LUMO}, and Δ_{H-L} are affected by the introduction of different donor group to 4-(4-phenyl-4-α-naphthylbutadieny)-triphenylamine.

To further study substituent effect, the contribution of substituent groups to HOMO and LUMO of the six molecules are further analyzed and relevant data are also listed in Table 1. From Table 1, we can find that substituents -$N(CH_3)_2$ and -C_6H_5 have the largest contribution to HOMO and LUMO, respectively, and H has the smallest contribution to HOMO and LUMO in all substituent groups. The sequence of contribution value to HOMO is -$N(CH_3)_2$>-C_6H_5>-OCH_3>-OH>-CH_3>H and LUMO is in the order of -C_6H_5>-$N(CH_3)_2$>-OCH_3>-OH>-CH_3>H. These results also indicate that the stronger electron-donating ability is, the bigger contribution to HOMO and LUMO is. Otherwise, it is also found that the contribution of substituent groups to HOMO is much bigger than that of LUMO. Therefore, it is clear to see that substitution of 4-(4-phenyl-4-α-naphthylbutadieny)-triphenylamine with electron-donating substituent makes the molecule more effective in hole transport than electron transport.

3.2 Absorption spectrum and stokes shift

To gain an insight into the electronic transition and excitation properties, the absorption and emission properties were characterized using the CAM-TD-B3LYP method on the optimized ground and excited states geometries, respectively. The

solvent effect for investigated system was considered in this work. Figure 3 shows the absorption spectrum. The absorption wavelengths (λ_{abs}) and emission wavelengths (λ_{em}) of molecules 1 - 6 are listed in Table 2. The λ_{abs} of molecules 1 - 6 are 381, 384, 384, 387, 387, and 397 nm, respectively, corresponding to dominant transition from HOMO to LUMO (1: 88%, 2: 83%, 3: 86%, 4: 83%, 5: 84%, 6: 75%). The trend of λ_{abs} value is 6>5=4>3=2>1, the λ_{abs} of molecules 2 – 6 have slight bathochromic shifts compared with that of 1. In other words, the stronger electron-donating ability is, the larger the λ_{abs} of molecule is. For all molecules, the π-π* transition feature around 380-400 nm is presented. It can be seen from Table 2 that molecules 2 - 6 have larger oscillator strength than that of molecule 1. The sequence is 2>6>4>5>3>1. f_{abs} strength for an electronic transition is proportional to the transition dipole moment. The result shows that molecules 2 - 6 have larger absorption intensity than that of molecule 1.

The λ_{em} of molecules 1 - 6 are 490, 488, 487, 479, 480, and 474 nm, respectively, which indicates that λ_{em} of molecules 2 – 6 have slight blue shifts compared with that of molecule 1, the deviations are 2, 3, 11, 10, and 16 nm, respectively. In addition, it is also found that the emission spectrums of molecules 1 – 6 show a large Stokes shift of 109, 104, 103, 92, 93, and 97 nm, respectively. Prof. Mhaisalkar and Grimsdale anticipated that the large Stokes shift, lower glass transition temperature and smaller molecule size versus spiro-OMeTAD would be synergistically beneficial in the infiltration and pore-filling of a hole-transporting material for perovskites-type solar cells by simple annealing or light soaking posttreatment[33]. The large stokes shift

reflects the big structure difference between ground and excited states of molecule, which indicates that the molecule may be flexible. Perhaps it is beneficial in pore-filling of a hole-transporting material. For this reason we conjecture that molecules 1, 2, and 3 are more favorable for improving power conversion efficiency than 4, 5, and 6.

3.3 Reorganization energy, electron affinity, and ionization potential

Reorganization energy is one of the key parameter to determine the carrier hopping rate. It comes from contributions of external reorganization energy and internal reorganization energy. As is known that the external reorganization energy is quite smaller than the inner part based on a polarized force field calculation[34], and thus external part is not considered in this research. The calculated reorganization energies for hole and electron are listed in Table 3. From Table 3, we can find that the λ_h of molecules 1 – 6 (1: 0.14 eV, 2: 0.12 eV, 3: 0.12 eV, 4: 0.10 eV, 5: 0.10 eV, 6: 0.16 eV) are much smaller than that of a typical hole transport material N,N'-diphenyl-N,N'-bis(3-methylphenyl)-(1,1'-biphenyl)-4,4'-diamine (TPD) with λ_h=0.29 eV. This means that their hole transfer rate should be higher than that of TPD, and compared with TPD molecules 1 – 6 could be good hole transfer materials from the λ_h, In addition, for 4-(4-phenyl-4-α-naphthylbutadieny)-triphenylamine with the electron releasing group, the substituent effect for reorganization energy has the following order: 6 > 1 > 2 = 3 > 4 = 5. This is to say that the λ_h values of molecules 1 to 5 are decreasing with the increasing of electron-donating ability of substituent groups. But molecule 6 is a particular case, although it contains the substituent group

with the strongest electron-donating ability, it has the biggest λ_h in all molecules. The reason may be that nitrogen atom has bigger electronegativity than oxygen and carbon atom and the lone pair electrons of nitrogen atom is undesirable for the stability of molecule 6 in neutral and charged species in their lowest energy geometries. For λ_e, it is found that the effect of the substituent is not pronounced, and the λ_h of all molecules are bigger than λ_e, which implies that the hole mobility is larger than the electron mobility.

The stability is also a useful criterion to evaluate the nature of devices for carries transport materials. To our knowledge, the adiabatic ionization potential (IP_a) is directly relevant to the stability of p-type materials. From the IP_a given by Table 3, molecule 1 (4.77eV) has the biggest IP_a value and 6 (4.25eV) has the smallest IP_a value compared with other four molecules. Additionally, the IP_a values of molecules 1 – 6 decrease as electron-donating ability increase. Furthermore, the absolute hardness (η) also has been calculated using operational definition [35, 36] given by: η=(IP-EA)/2. The η is the resistance of the chemical potential to change in the number of electrons. The η values of all molecules are also listed in Table 3. From Table 3 we can find that molecules 1 – 5 have similar stability, while 6 has smallest η value, which indicates that molecule 6 has a poor stability in all molecules.

3.4 Exciton binding energies and hole mobilities

To achieve high efficiencies, the bound electron-hole pairs should be dissociated into the fully separated positive and negative charges to escape from the coulomb attraction. It is directly related to the charge separation in solar cells. The exciton

binding energy (E_b) is defined as the potential energy difference between the neutral singlet exciton and two free charge carriers, and it can be expressed as [37, 38]: $E_b=E_g-E_x=\Delta_{H-L}-E_1$. The E_g is the electronic band gap and can be replaced by the energy gap (Δ_{H-L}), and E_x is the optical gap and is generally defined as the first singlet excitation energy (E_1). The relevant data are listed in Table 4. From Table 4, we can see that the trend of E_b is 1>2=3>5>4>6, and this shows that the stronger electron-donating ability is, the easier the separation of electron-hole pairs escape from coulomb attraction is. From the value of E_b, we can conjecture that introduction of electron releasing groups can efficiently improve carrier (hole and electron) mobility.

The calculated crystal structures of all molecules with the total energies belong to space groups P21/C. Thus, we predict the hole mobilities of molecules 1 - 6 in P21/C. Recently, Hui-xue Li and coworkers[16] have verified the reliability of the predicted crystal structures by compassion experimental crystal structures. Their result shows that the predicted packing structure is the same with dinaphtho-tetrathiafulvalene (DN-TTF) except for the volume and density of the unit cell. So we think that the method of predicted crystal structures is reliable for molecules 1-6. We arbitrarily choose one molecule in the crystal as the carrier donor and take all its neighboring molecules as paired elements. Each pair is defined as a transmission path. Figure 4 shows the most important pathways. Here, we neglected some pathways with transfer integrals less than 1 meV, which make little contribution to mobility. Transfer integral is important for determining charge carrier mobility. It represents the orbital coupling

of the neighboring molecules. The value of transfer integrals is also dependent on the relative position of interacting molecules and their FMO distribution patterns [39]. The M06-2X functional is a highnonlocality functional with double the amount of nonlocal exchange (2X), and it is parametrized only for nonmetals. Donald G. Truhlar has pointed out that M06-2X is the best functional for noncovalent interactions by comparing 12 other functionals and Hartree–Fock theory[40]. In addition, Zhong-Min Su also proved that the M06-2X/6-31G(d,p) can provide a better description of the non-covalent interaction than the PW91PW91 functional[41]. Thus, M06-2X functional was employed to calculate the transfer integrals of all hopping pathways based on the direct coupling approach. Combining the Marcus formula with the Einstein relation, the hole mobilities of molecules 1 - 6 based on their crystal structures are obtained. The centroid to centroid distance of dimer, the hole transfer integrals, hole hopping rates, and hole mobilities of main hopping pathway are listed in Table 5. From the *u* of molecules 3 and 4 given by Table 5, it is found that the calculated *u* (the calculated *u* of molecules 3 and 4 are 0.0600 and 0.0483 $cm^2v^{-1}s^{-1}$, respectively.) has a same trend as experimental (the experimental *u* of molecules 3 and 4 are 2.98×10^{-3} and 1.27×10^{-3} $cm^2v^{-1}s^{-1}$, respectively.), which indicates that it is reliable to have a qualitative comparison between the experimental values and the theoretical results at present theoretical level. It is worth noting that the theoretical method we used to describe charge transport is based on some sound approximations and assumptions, so the accurate absolute hole mobility is not the aim of this work. Importantly, the aim of this work is to reveal the structure-property relationship and look for excellent HTM

with high hole mobility to further develop efficient perovskites-type solar cells. From Table 5, we can find that molecule 2 has the biggest hole mobility (0.1063 $cm^2v^{-1}s^{-1}$) due to large hole transfer integral and hole hopping rate, which is favorable for obtaining high performance carrier transport material, and the face-to-face stacking also increases the effective π-orbital overlap and enhances the hole mobility between conjugated molecules. The molecule 6 has the smallest hole mobility (0.0011 $cm^2v^{-1}s^{-1}$). Prof Snaith and Grätzel pointed out that the HTMs containing N atom with the low hole mobility is by the sp^3 hybridization of the N atom, the inherent triangular pyramid configuration leads to large intermolecular distance, thus suffer from low hole mobility, low conductivity, or both in their pristine form[42, 43]. However, our results show that the intermolecular distance of molecule 6 is shortest except for the pathway 2 and 4 of molecule 5 in all molecules. So, we conjecture that the low hole mobility of molecule 6 originates from two possible reason: larger reorganization energy and cross packing of dimer. In addition, it is found that molecules 1 and 4 have similar packing mode leading to a very similar hole mobility. From Figure 4 and Table 5, we know that among all selected pathways, the largest transfer integral of all investigated systems corresponds to molecule 2 (such as pathway 1) with the slipped π–π packing. This finding further proves the traditional view that the pathway with cofacial π–π packing in general possesses relatively larger transfer integral than other pathway with edge-to-face (such as pathway 4 of molecule 3), edge-to-edge stacking (such as pathway 1 and 3 of molecule 5), or cross packing (such as pathway 1 and 2 of molecule 6). From molecules 1 to 6, the hole mobilities have not showed regular

changes as electron-donating ability of substituent group increased.

As point out above, π–π packing mode of dimer plays an important role in determining hole mobility, and substituent $–C_6H_5$ is a better substituent group in improving hole mobility than those of $–OCH_3$ and $-CH_3$, which are popular substituent group experimentally for HTMs. As discussed above, we hope that our results are helpful for design of high efficient HTMs in perovskites-type solar cells.

4. Conclusions

We have presented a theoretical investigation based upon DFT and TD-DFT calculations aimed to elucidate what the effects of introducing substituents of different electron-donating ability on the crystal packing and transport properties of 4-(4-phenyl-4-α-naphthylbutadieny)-triphenylamine derivatives. The electronic structures, transfer integrals, reorganization energies, exciton binding energies and hole mobilities are discussed, summarized as follows:

(1) The FMOs analysis results show that they have similar distribution to the frontier orbitals where the HOMOs are delocalized over the entire molecule while their LUMOs are not fully delocalized throughout the whole molecule, and the stronger electron-donating ability is, the bigger contribution to HOMO and LUMO is. Moreover, the electron releasing substituents increase the HOMO and LUMO energies of all molecules.

(2) Spectrum analysis indicates that the λ_{abs} of molecules 1 - 6 corresponds to dominant transition from HOMO to LUMO, and all compounds have large Stokes shift based on absorption and emission spectrums.

(3) Moreover, the λ_h of all molecules are bigger than λ_e, which implies that the hole mobility is larger than electron, and we can also find that molecules 1 – 5 have similar stability, molecule 6 has the most poor stability in all molecules from the viewpoint of absolute hardness.

(4) The hole mobilities of molecules 1 - 6 in space ground P21/C are 0.0465, 0.1063, 0.0600, 0.0483, 0.0221, and 0.0011 $cm^2v^{-1}s^{-1}$, respectively, which indicates that phenyl is an outstanding substituent group for improving hole mobility comparison with methoxyl and methyl. And π–π packing mode plays an important role in determining hole mobility.

It is our expectation that our research findings could give a hand to researchers who design and develop high performance hole transport materials for perovskites-type solar cells.

Acknowledgements

This work is financially supported by the Major State Basic Research Development Programs of China (2011CBA00701), the National Natural Science Foundation of China (21473010, 21303007), the Excellent Young Scholars Research Fund of Beijing Institute of Technology (2013YR1917), and Beijing Key Laboratory for Chemical Power Source and Green Catalysis (2013CX02031). This work is also supported by the opening project of State Key Laboratory of Explosion Science and Technology (Beijing Institute of Technology) (ZDKT12-03)

References

1. A. Kojima, K. Teshima, Y. Shirai and T. Miyasaka, *J Am Chem Soc*, 2009, **131**, 6050-6051.
2. J. H. Im, C. R. Lee, J. W. Lee, S. W. Park and N. G. Park, *Nanoscale*, 2011, **3**, 4088-4093.
3. H.-S. Kim, C.-R. Lee, J.-H. Im, K.-B. Lee, T. Moehl, A. Marchioro, S.-J. Moon, R. Humphry-Baker, J.-H. Yum and J. E. Moser, *Sci Rep*, 2012, **2**.
4. M. M. Lee, J. Teuscher, T. Miyasaka, T. N. Murakami and H. J. Snaith, *Science*, 2012, **338**, 643-647.
5. N. J. Jeon, H. G. Lee, Y. C. Kim, J. Seo, J. H. Noh, J. Lee and S. I. Seok, *J Am Chem Soc*, 2014, **136**, 7837-7840.
6. J. Shi, J. Dong, S. Lv, Y. Xu, L. Zhu, J. Xiao, X. Xu, H. Wu, D. Li and Y. Luo, *Appl. Phys. Lett.*, 2014, **104**, 063901.
7. J. Liu, W. Yongzhen, C. Qin, X. Yang, T. Yasuda, A. Islam, K. Zhang, W. Peng, L. Han and W. Chen, *Energy Environ Sci*, 2014.
8. P. Qin, S. Paek, M. I. Dar, N. Pellet, J. Ko, M. Grätzel and M. K. Nazeeruddin, *J Am Chem Soc*, 2014, **136**, 8516-8519.
9. A. Krishna, D. Sabba, H. Li, J. Yin, P. P. Boix, C. Soci, S. G. Mhaisalkar and A. C. Grimsdale, *Chem Sci*, 2014, **5**, 2702-2709.
10. S. Lv, L. Han, J. Xiao, L. Zhu, J. Shi, H. Wei, Y. Xu, J. Dong, X. Xu, D. Li, S. Wang, Y. Luo, Q. Meng and X. Li, *Chem Commun*, 2014, **50**, 6931-6934.
11. M. C. R. Delgado, E.-G. Kim, D. A. d. S. Filho and J.-L. Bredas, *J Am Chem Soc*, 2010, **132**, 3375-3387.
12. M.J. Frisch, G. W. Trucks, H.B. Schlegel, G.E. Scuseria, M.A. Robb,, G. S. J.R. Cheeseman, V. Barone, B. Mennucci, G.A., H. N. Petersson, M. Caricato, X. Li, H.P. Hratchian, A.F., J. B. Izmaylov, G. Zheng, J.L. Sonnenberg, M. Hada, M., K. T. Ehara, R. Fukuda, J. Hasegawa, M. Ishida, T. Nakajima,, O. K. Y. Honda, H. Nakai, T. Vreven, J. Montgomery, J. A., J.E., F. O. Peralta, M. Bearpark, J.J. Heyd, E. Brothers, K.N., V. N. S. Kudin, R. Kobayashi, J. Normand, K., A. R. Raghavachari, J.C. Burant, S.S. Iyengar, J. Tomasi, M., N.

R. Cossi, J.M. Millam, M. Klene, J.E. Knox, J.B. Cross, V., C. A. Bakken, J. Jaramillo, R. Gomperts, R.E. Stratmann, O., A. J. A. Yazyev, R. Cammi, C. Pomelli, J.W. Ochterski, R.L., K. M. Martin, V.G. Zakrzewski, G.A. Voth, P. Salvador, J.J., S. D. Dannenberg, A.D. Daniels, O. Farkas, J.B. Foresman, and J. C. J.V. Ortiz, D.J. Fox, Gaussian 09W Revision B.02.

13. T. Yanai, D. P. Tew and N. C. Handy, *Chem Phys Lett*, 2004, **393**, 51-57.
14. A. Troisi, *Adv Mater*, 2007, **19**, 2000-2004.
15. M. E. Gershenson, V. Podzorov and A. F. Morpurgo, *Rev Mod Phys*, 2006, **78**, 973-989.
16. H. X. Li, R. H. Zheng and Q. A. Shi, *Phys Chem Chem Phys*, 2011, **13**, 5642-5650.
17. G. R. Hutchison, M. A. Ratner and T. J. Marks, *J Am Chem Soc*, 2005, **127**, 16866-16881.
18. G. Nan and Z. Li, *Phys Chem Chem Phys*, 2012, **14**, 9451-9459.
19. G. Nan and Z. Li, *Org Electron*, 2012, **13**, 1229-1236.
20. C. H. Li, C. H. Huang and M.-Y. Kuo, *Phys Chem Chem Phys*, 2011, **13**, 11148-11155.
21. R. A. Marcus, *Rev Mod Phys*, 1993, **65**, 599-610.
22. M. Malagoli and J. L. Brédas, *Chem Phys Lett*, 2000, **327**, 13-17.
23. V. Lemaur, D. A. da Silva Filho, V. Coropceanu, M. Lehmann, Y. Geerts, J. Piris, M. G. Debije, A. M. van de Craats, K. Senthilkumar, L. D. A. Siebbeles, J. M. Warman, J.-L. Brédas and J. Cornil, *J Am Chem Soc*, 2004, **126**, 3271-3279.
24. E. F. Valeev, V. Coropceanu, D. A. da Silva Filho, S. Salman and J.-L. Brédas, *J Am Chem Soc*, 2006, **128**, 9882-9886.
25. S. Yin, Y. Yi, Q. Li, G. Yu, Y. Liu and Z. Shuai, *J Phys Chem A*, 2006, **110**, 7138-7143.
26. A. Troisi and G. Orlandi, *Chem Phys Lett*, 2001, **344**, 509-518.
27. L. Schein and A. McGhie, *Phys Rev B*, 1979, **20**, 1631.
28. X. Yang, Q. Li and Z. Shuai, *Nanotechnology*, 2007, **18**, 424029.

29. C. Materials Studio; Accelrys; San Diego, 2005.
30. S. L. Mayo, B. D. Olafson and W. A. Goddard, *J Phys Chem*, 1990, **94**, 8897-8909.
31. A. N. Sokolov, S. Atahan-Evrenk, R. Mondal, H. B. Akkerman, R. S. Sánchez-Carrera, S. Granados-Focil, J. Schrier, S. C. B. Mannsfeld, A. P. Zoombelt, Z. Bao and A. Aspuru-Guzik, *Nat Commun*, 2011, **2**, 437.
32. B. Zhang, Y.-H. Kan, Y. Geng, Y.-A. Duan, H.-B. Li, J. Hua and Z.-M. Su, *Org Electron*, 2013, **14**, 1359-1369.
33. H. Li, K. Fu, A. Hagfeldt, M. Grätzel, S. G. Mhaisalkar and A. C. Grimsdale, *Angew Chem Int Ed*, 2014, **53**, 4085-4088.
34. J. E. Norton and J.-L. Brédas, *J Am Chem Soc*, 2008, **130**, 12377-12384.
35. R. G. Pearson, *J Am Chem Soc*, 1985, **107**, 6801-6806.
36. M. S. Stark, *J Phys Chem A*, 1997, **101**, 8296-8301.
37. Y. Li, T. Pullerits, M. Zhao and M. Sun, *J Phys Chem C*, 2011, **115**, 21865-21873.
38. G. D. Scholes and G. Rumbles, *Nat Mater*, 2006, **5**, 920-920.
39. J. L. Bredas, D. Beljonne, V. Coropceanu and J. Cornil, *Chem Rev*, 2004, **104**, 4971-5003.
40. Y. Zhao and D. G. Truhlar, *Theore Chem Acc*, 2008, **120**, 215-241.
41. Y. Geng, S.-X. Wu, H.-B. Li, X.-D. Tang, Y. Wu, Z.-M. Su and Y. Liao, *J Mater Chem*, 2011, **21**, 15558-15566.
42. J. Burschka, A. Dualeh, F. Kessler, E. Baranoff, N.-L. Cevey-Ha, C. Yi, M. K. Nazeeruddin and M. Grätzel, *J Am Chem Soc*, 2011, **133**, 18042-18045.
43. T. Leijtens, J. Lim, J. Teuscher, T. Park and H. J. Snaith, *Adv Mater*, 2013, **25**, 3227-3233.

Table 1. The FMOs energies of E_{HOMO} (eV), E_{LUMO} (eV), and Δ_{H-L} (eV), and HOMOs and LUMOs contribution of substituent groups (SG) fragments (in %) to FMOs of molecules at B3LYP/6-31G(d,p) level.

Compounds	HOMO		LUMO		Δ_{H-L}
	E_{HOMO}	SG	E_{LUMO}	SG	
1	-4.84	0.028	-1.68	0.008	3.16
2	-4.82	5.59	-1.75	1.25	3.07
3	-4.76(-5.35)	1.14	-1.69(-2.60)	0.13	3.07(2.75)
4	-4.65(-5.23)	4.58	-1.64(-2.60)	0.22	3.01(2.63)
5	-4.66	3.52	-1.64	0.19	3.02
6	-4.65	15.56	-1.57	0.35	3.08

Note: The experimental data in brackets is from Ref [10]

Table 2. The absorption wavelengths λ_{abs} and emission wavelengths λ_{em} of molecules 1-6 based on the S_0 and S_1 states, respectively, along with Stokes shift at CAM-TD-B3LYP/6-31G** level.

Compounds	Absorption			Emission	Shift
	λ_{abs}	f_{abs}	assignments	λ_{em}	
1	381	1.72	H-0->L+0(88%)	490	109
2	384	1.84	H-0->L+0(83%)	488	104
3	384	1.74	H-0->L+0(86%)	487	103
4	387	1.78	H-0->L+0(83%)	479	92
5	387	1.77	H-0->L+0(84%)	480	93
6	397	1.82	H-0->L+0(75%)	474	97

Table 3 Internal hole/electron reorganization energies (λ_h/λ_e, eV), adiabatic ionization potential (IP_a, eV), and electron affinities (EA_a, eV) calculated at B3LYP/6-31G** level.

Compounds	λ_h	λ_e	IP_a	EA_a	η
1	0.14	0.23	4.77	1.87	1.45
2	0.12	0.22	4.76	1.91	1.43
3	0.12	0.23	4.71	1.84	1.44
4	0.10	0.24	4.62	1.81	1.41
5	0.10	0.23	4.63	1.81	1.41
6	0.16	0.24	4.25	1.75	1.25

Table 4. Calculated the first singlet excitation energy (E_1, eV) and exciton binding energies at B3LYP/6-31G(d,p) level.

compounds	E_1	E_b
1	2.53	0.72
2	2.54	0.68
3	2.54	0.68
4	2.59	0.61
5	2.58	0.62
6	2.61	0.47

Table 5. The centroid to centroid distances (d, Å), the hole transfer integrals t_{ij} (meV), hole hopping rate k_{ij} (s^{-1}), and hole mobilities (u, $cm^2v^{-1}s^{-1}$) of main hopping pathways selected based on the predicted crystalline structures.

Compound	pathway	d	t_{ij}	k_{ij}	u
1	1	9.734	8.84	8.98×10^{11}	0.0465
	2	8.807	5.06	2.94×10^{11}	
	3	9.542	4.51	2.34×10^{11}	
	4	9.934	8.84	8.98×10^{11}	
2	1	6.897	15.4	3.57×10^{12}	0.1063
	2	14.042	2.87	1.24×10^{11}	
3	1	14.408	1.29	2.51×10^{10}	0.0600 (2.98×10^{-3})[a]
	2	7.791	4.26	2.74×10^{11}	
	3	10.359	3.44	1.78×10^{11}	
	4	10.359	3.43	1.78×10^{11}	
	5	7.455	11.8	2.10×10^{12}	
4	1	8.480	3.92	3.08×10^{11}	0.0483 (1.27×10^{-3})[a]
	2	8.487	3.92	3.08×10^{11}	
	3	14.056	5.65	6.40×10^{11}	
	4	10.090	6.14	7.57×10^{11}	
	5	8.964	1.22	2.99×10^{11}	
5	1	10.459	1.68	5.57×10^{10}	0.0221
	2	5.609	7.78	1.24×10^{12}	
	3	10.466	1.61	5.57×10^{10}	
	4	5.709	6.94	9.67×10^{11}	
6	1	6.132	2.23	4.36×10^{10}	0.0011
	2	6.129	2.22	4.36×10^{10}	

[a] Experimental data are obtained from Ref [10].

Figure 1. Chemical structure and name of studied molecules, the hydrogen atoms and corresponding C-H bonds have been omitted for clarity. The molecular name is replaced by corresponding number in brackets.

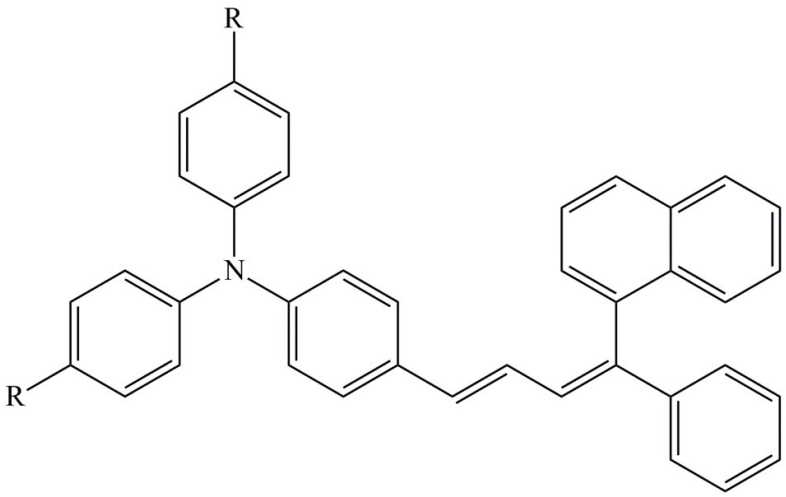

R= -H (1)

R= -C_6H_5 (2)

R= -CH_3 (3)

R= -OCH_3 (4)

R= -OH (5)

R= -$N(CH_3)_2$ (6)

Figure 2. Illustration of frontier molecules orbitals for molecules 1 - 6 at B3LYP/6-31G** level.

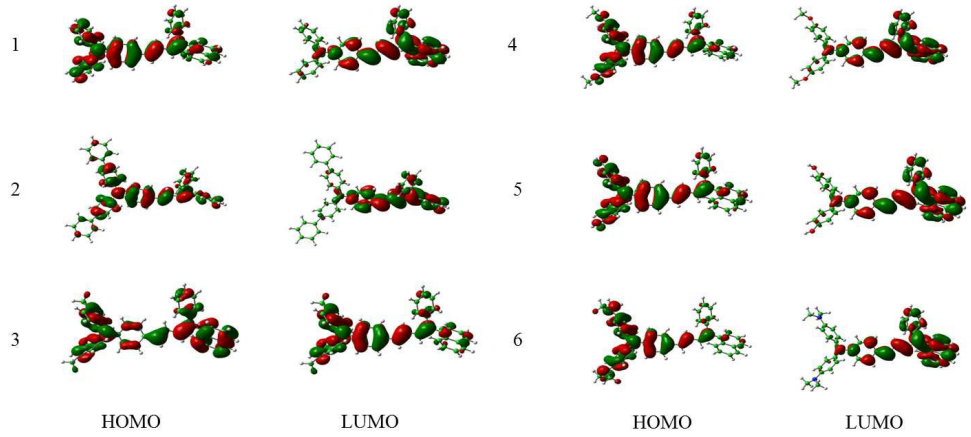

Figure 3. The calculated absorption of molecules 1 - 6 at CAM-TD-B3LYP/6-31G** level in chlorobenzene.

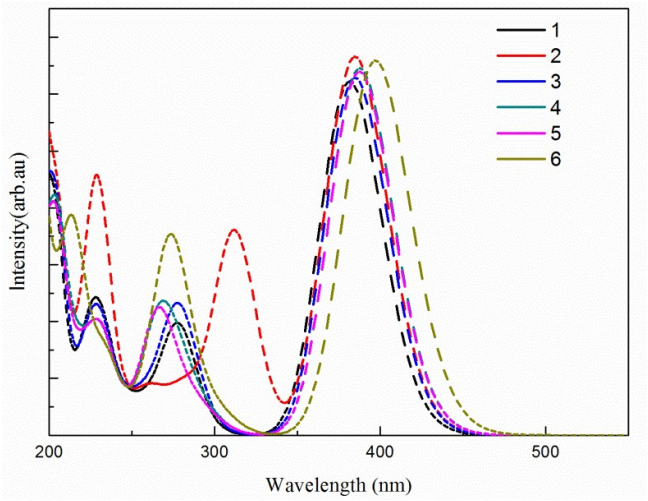

Figure 4. Main hole hopping pathways selected based on the predicted crystal structures for molecules 1 - 6.